sciendo

BULGARIAN ACADEMY OF SCIENCES

CYBERNETICS AND INFORMATION TECHNOLOGIES • Volume **20**, No 6
Special Issue on New Developments in Scalable Computing
Sofia • 2020 Print ISSN: 1311-9702; Online ISSN: 1314-4081
DOI: 10.2478/cait-2020-0061

Evaluating Machine Learning Approaches for Discovering Optimal Sets of Projection Operators for Quantum State Tomography of Qubit Systems

Violeta N. Ivanova-Rohling[1], *Niklas Rohling*[2]

[1]*Department of Physics and Zukunftskolleg, University of Konstanz, Germany and Department of Mathematical Foundations of Computer Sciences, Institute of Mathematics and Informatics, Bulgarian Academy of Sciences, Akad. G. Bonchev Str., Bl. 8, 1113 Sofia, Bulgaria*
[2]*Department of Physics, University of Konstanz, Germany*
E-mails: violeta.ivanova-rohling@uni-konstanz.de niklas.rohling@uni-konstanz.de

Abstract: *Finding optimal measurement schemes in quantum state tomography is a fundamental problem in quantum computation. It is known that for non-degenerate operators the optimal measurement scheme is based on mutually unbiassed bases. This paper is a follow up from our previous work, where we use standard numerical approaches to look for optimal measurement schemes, where the measurement operators are projections on individual pure quantum states. In this paper we demonstrate the usefulness of several machine learning techniques – reinforcement learning and parallel machine learning approaches, to discover measurement schemes, which are significantly better than the ones discovered by standard numerical methods in our previous work. The high-performing quorums of projection operators we have discovered have complex structure and symmetries, which may imply that the optimal solution will possess such symmetries.*

Keywords: *Quantum information, optimization problem, Widening, reinforcement learning.*

1. Introduction

1.1. Quantum state tomography in d dimensions with projective measurements

While pure quantum states are represented by normalized vectors in a Hilbert space of complex dimension d, interaction with an environment can lead to mixed states represented by a Hermitian trace-1 $d\times d$-matrix ρ, thus, ρ is given by d^2-1 real parameters. Quantum State Tomography (QST) is the procedure to determine these parameters. Projective quantum measurements, represented by Hermitian $d\times d$-matrix have up to d different outcomes, the eigenvalues of such a matrix. We write the

measurement operator as $\sum_j \lambda_j P_j$ where λ_j are the eigenvalues and P_j are projection operators. The probability to measure λ_j, is given by the trace of the matrix product of ρ and P_j, $\mathrm{Tr}(\rho P_j)$. Repetitions of a measurement are needed in order to obtain an estimate for these probabilities by the frequencies of the measurement outcomes. As one projective measurement provides no more than d–1 parameters, different measurements are needed. We focus on the question what is an ideal choice of measurements under certain restriction in the sense that we want to find the minimal set of measurement operators (quorum) that allows for estimating ρ with a desired precision with as little measurements as possible.

The importance of QST lies in the possibility to demonstrate full control over the system and to verify the functionality of a quantum device, and to debug it. Consequently, QST has been performed for many quantum mechanical systems intended as building blocks of a quantum computer [1-4].

1.2. SIC-POVMs as an alternative approach

A generalized quantum measurement is expressed by a Positive Operator-Valued Measure (POVM). This is a set of positive semi-definite matrices F_j that fulfill $\sum_j F_j = I_d$ where I_d is the $d \times d$ unity matrix. Using an ancilla quantum system, the measurement can have more than d different outcomes, each of them has the probability $\mathrm{Tr}(F_j \rho)$. For QST with one repeated generalized measurement, the corresponding POVM needs to be informationally complete. Then it has to have at least d^2 elements.

Symmetric, Informationally Complete POVMs (SIC-POVMs) are of great importance for QST due to their beneficial properties and the fact that they seem to be available for all d [5, 6, 7]. SIC-POVMs are formed by d^2 quantum states $|\psi_j\rangle$, which fulfill $|\langle\psi_j|\psi_k\rangle|^2 = 1/(d+1)\ \forall\ j \neq k$, and then the elements of the POVM are proportional to the projectors on these states, $F_j = |\psi_j\rangle\langle\psi_j|/d$.

2. Optimized quantum state tomography as optimization problem

2.1. Geometric quality measure

As the trace of ρ is known, we work in the (d^2-1)-dimensional vector space of traceless $d \times d$-matrices with the inner product defined as $\langle A|B\rangle = \mathrm{Tr}(A^\dagger B)$ for $d \times d$-matrices A and B, where $A^\dagger$ is the conjugate transposed of A and $\mathrm{Tr}(A^\dagger B)$ is the trace over the matrix product of $A^\dagger$ and B. For the projectors involved in our QST quorum we define their traceless part as

$$Q_j = P_j - \mathrm{rank}(P_j)\, \mathrm{I}_d / d. \tag{1}$$

Wootters and Fields [8] showed that the information gain by quantum measurements with a fixed number of repetitions becomes maximal if the volume spanned by the d^2-1 linear independent Q_j is maximal. We can express this volume as

$$|\det Q| = |\det(Q_1 |Q_2 |\ldots|Q_{d^2-1})|, \tag{2}$$

where Q is the $(d^2-1)\times(d^2-1)$-matrix with the columns representing the Q_j as coefficients for a basis of the (d^2-1)-dimensional vector space.

2.2. Non-degenerate measurements

Wootters and Fields [8] considered the non-degenerate case, where each measurement has d different eigenvalues. Consequently, to determine ρ, d+1 different measurements need to be performed. Wootters and Fields found that ideally the different measurements are informationally independent or *mutually unbiased*, meaning that results from one of the measurements do not provide any prediction for the outcome of the other measurements. Mathematically speaking this is the case if $\langle Q_j|Q_m \rangle = 0$ for all j, m from different measurements. Note that one cannot change the value $\langle Q_j|Q_m \rangle = -1/d$ for j, m being from the same basis, as the respective quantum states are orthogonal to each other. The eigenbases of the measurement operators are then called Mutually Unbiased Bases (MUBs). A complete set of $d + 1$ MUBs exists if d is a prime power [8], e.g., for K qubits, $d = 2^K$.

2.3. Projection on half-dimensional subspaces

If in a composite quantum system only one qubit can be measured, this is represented by independent rank – $d/2$ projectors. For d being of prime-power dimension d^2-1 of those half-dimensional projectors can be arranged in an optimal fashion [9], i.e., $\langle Q_j|Q_m\rangle = 0 \; \forall \; j \neq m$.

2.4. Rank-1 projectors in d-dimensional Hilbert space

We now consider measurements that distinguish between one quantum state and the remaining $(d – 1)$-dimensional subspace, describe by rank-1 projectors. For two spin qubits in semiconductor quantum dots, rank-1 projectors can be realized by spin-to-charge readout [10, 11]. While we deal with d^2-1 rank-1 projectors as Wootters and Fields [8] did, they are now completely independent. Each has to be realized by a different measurement. One can choose to rebuild the projectors on states from sets of MUBs [10]. However, by numerical optimization, we showed [11] that this is not the optimal choice.

Furthermore, one can proof that the Q_j cannot be arranged all orthogonal to each other in this situation if $d > 2$. A proof is given in [10] for $d = 4$ and can be generalized for other dimensions. As an alternative one can drop the condition of forming a minimal set and instead project one-by-one on the states forming a SIC-POVM. For $d = 4$, we have shown by simulating QST that this outperforms the numerically optimized minimal QST schemes [11].

3. Three-qubit system, $d = 8$

We focus on the case of three qubits, $d = 8$ because the optimization problem becomes more challenging with increasing dimension. For two qubits, Powell's method applied in [11], seemed to find the optimal value of the quality measure $|\det Q|$ in a reliable way, for three qubits this was not the case.

We need to find a quorum of 63 projectors P_j on quantum states $|\psi_j\rangle$, i.e., in bra-ket notation $P_j=|\psi_j \rangle\langle\psi_j|$. Each quantum state, i.e., normalized vectors of arbitrary

global phase, in an 8-dimensional complex Hilbert space is parametrized via $|\psi_j\rangle = x_j^k |k\rangle$, with $\{|k\rangle, k = 0, \ldots,7\}$ being a basis of the Hilbert space, by

$$x_j^k = \exp(i\,\varphi_k^j)\cos\theta_k^j \prod_{l=0}^{k-1}\sin\theta_l^j \tag{3}$$

with $\varphi_0^j = 0$ and $\theta_7^j = 0$. So that for each state j, we need to know the 14 parameters $\{\theta_0^j, \ldots, \theta_6^j, \varphi_1^j, \ldots, \varphi_7^j\}$. The quality measure $|\det Q|$ is invariant under unitary operations applied to all quantum states. Thus, we can choose some of the parameters without loss of generality. Namely, we can choose for the first eight states: $\varphi_k^j = 0\ \forall\ k \geq j$ and $\theta_k^j = 0\ \forall\ k \geq j$. The number of remaining free parameters is 819. From the volume of a hypercube we obtain the non-reachable upper bound, $(7/8)^{63/2} = 0.01490$. As a starting point we choose, for simplicity, random values for $\varphi_k^j \in [0, 2\pi)$ and $\theta_k^j \in [0, \pi/2)$. For comparison, the best result found in [11] was $|\det Q| = 0.001803$.

4. General Widening

Most research in parallel data mining focuses on the processing of larger data sets or the speed-up of existing algorithms.

Yet for many tasks, it is the quality of result obtained by the algorithm, which is of the greatest importance. Often data mining algorithms employ a greedy heuristic, which relies on the local optimality property in order to make the search through an enormous space of potential solutions feasible.

Due to this limited exploration, finding the optimal solution is not guaranteed. In [12], a strategy for using parallel resources to improve the results obtained by a greedy heuristic, while at the same time keeping the running time constant, is proposed. This strategy is referred to by the authors as *Widening*. The goal of Widening is to invest the available parallel resources in multiple simultaneous searches through the solution space and, by that, it achieves an improvement of the solution quality. In order to invest the parallel resources intelligently, it is critical to avoid the exploration of very similar solutions in parallel and converging to a local optimum. Diversity needs to be used in order to force the widened search to investigate the solution space more broadly. In [13] a more in-depth discussion of the importance of diversity in Widening is presented, introducing the concept of *diversity-driven Widening*. In [14, 15] neighborhood-based Widening approaches were developed. A greedy data mining heuristic can be presented as a search through the space of models from M. At each step the greedy algorithm chooses a locally optimal solution, until a sufficiently good solution is found, based on predefined stopping criteria.

The search can thus be formalized as an iterative application of two operators: *refinement r* and *selection s*. The refinement operator generates a set of more specific, potentially better, models (or new *refinements*): $r(m) = M^r$. The *selection operator s* uses a model evaluation function ψ to choose the locally best model from the set of all possible refinements M^r. One iterative step of the greedy search can be presented as: $m' = s_{\text{best}}(r(m))$ where $s_{\text{best}}(r(m)) = \text{argmax}_{m'' \in r(m)}\ \{\psi(m'')\}$. Fig. 1-(1) shows this representation of a Greedy Algorithm.

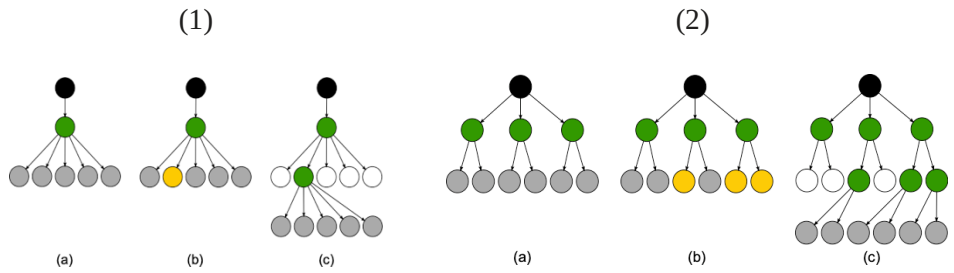

Fig. 1. Greedy Algorithm on the left (1): the current model m is depicted in green, the refinement options $r(m)$ are shown gray (a); the selection operator s picks the yellow refinement (b); the search continues from the chosen model (c). On the right (2) Widening is shown: From the set of current models (green), the refinement operator creates refinements (gray); a subset of the refined models (yellow circles in (b)) are selected and the search continues (c)

Using the abstract selection and refinement operators, a Widening of a greedy heuristic can be defined as a modification of the selection operator s,

(4) $$M' = \{m'_1, \ldots, m'_k\} = s_W(\bigcup_{m \in M} r(m)).$$

At each step, the selection operator s_W considers the refinements of a set M with of size k and returns a new set M' of k refined models. Fig. 1 (2) illustrates this process. In order to prevent convergence to local optimum we introduce diversity in the selection criteria by modifying the selection operator so that at each step it builds a set of best models that satisfy a diversity threshold δ to the already chosen models.

5. Powell's method

Powell's conjugate direction method [16] is a derivative-free algorithm for finding a local minimum of a real function. The method minimizes the function by a bi-directional search along each search vector, in turn. The bi-directional line search along each search vector can be done by Brent's method. The method is useful for calculating the local minimum of a continuous but complex function, especially one without an underlying mathematical definition, because it is not necessary to take derivatives. This is especially useful for our optimization problem. Furthermore, it is known that the Powell's method performs very well for exploitation, i.e., in situations where the starting point is not exceedingly far from the optimum. In [11], when comparing different standard numerical methods for optimization, Powell was the one, which performed the best without the necessity of additional parameter tuning. Due to its excellent exploitation properties, Powell's method has traditionally been combined with other algorithms, which perform very well for exploration, but not for exploitation. Our goal here is the same. We will take advantage of Powell's method strong abilities for local search, but try to generate excellent diverse starting points, which will help with the use of many Powell's searches explore the search space.

6. Parallelizing of the Powell's method

In order to improve the exploration of the search space we want to perform multiple Powell's searches in parallel. Due to the fact that Powell's method is very good in exploitation, the most important task and our focus is to find good starting points. We generate n starting points, which satisfy a chosen distance measure. We always maintain n number of parallel searches. If the distance between two solutions is smaller than the diversity threshold, the weaker solution is discarded. For each diverse solution discovered like this we look into their neighborhoods using the formula

$$x'_{mi} = x_{mi} + \varphi_{mi}(x_{mi} - x_{ki}), \tag{5}$$

where x_k, x_m are already discovered solutions, and $\varphi_{mi} \in [-1, 1]$; x'_m substitutes x_m in the set of starting points if it leads to a quorum of better quality. For each of the n points we generate n solutions at each step and pick the best n, which satisfy the diversity threshold. When the mean quality of the solutions stops improving, we use the discovered solutions as starting points of the Powell's method and we run n Powell's method searches in parallel, starting with high quality diverse starting points.

6.1. Diversity measures

We consider two different diversity measures, which capture different properties, meaningful for our problem. The first diversity measure tries to evaluate the Euclidean distance between the vectors of two quorums. The second diversity measure takes into consideration the invariance of the angles between the projectors in a quorum. The quality of a quorum is uniquely given by the pairwise angles. Namely if two different solutions have the same angles (or similar angles) we will consider them equivalent. Given two quorums $Q^{(1)} = \{Q'_1, Q'_2, \ldots, Q'_{63}\}$ and $Q^{(2)} = \{Q''_1, Q''_2, \ldots, Q''_{63}\}$, we calculate the angles that each projector vector $Q'_i \in Q^{(1)}$, $i = 1, \ldots, 63$, forms with $Q'_j \in Q^{(1)}$, $i = 1, \ldots, i-1, i+1, \ldots, 63$, and all the angles which $Q''_i \in Q^{(2)}$, $i = 1, \ldots, 63$, forms with $Q''_j \in Q^{(2)}$, $i = 1, \ldots, i-1, i+1, \ldots, 63$. We then calculate for each vector from $Q^{(1)}$ the similarity between the angles which each vector from $Q^{(2)}$ forms with the other projectors of $Q^{(2)}$. We calculate the mean common angles for each projector and divide it by 63 to normalize. This we use as a distance measure.

Calculating the Euclidean distance directly is infeasible, due to the size of the quorum (63) and the inability to know which projector from $Q^{(1)}$ to match to which projector to $Q^{(2)}$. Note that two quorums are identical if they contain the same elements in different order. That is why we use a modified Euclidean distance. This we calculate by ordering all projectors in a quorum based on their similarity to the fixed projector $Q_1^{(k)}$, which is present in each quorum. The fixed projector is the same in each quorum. We then calculate the Euclidean distance using the *sorted* quorums, by calculating the Euclidean distance of $Q'_i \in Q^{(1)}$ to $Q''_i \in Q^{(2)}$.

7. Reinforcement learning

Reinforcement learning is an area of machine learning, where an agent learns a behavior in a given environment, which maximizes the notion of cumulative reward. Reinforcement learning is one of three basic machine-learning paradigms, alongside supervised learning and unsupervised learning and is heavily used to solve complex optimization problems. It looks for optimal exploration and exploitation to solve a problem. Given an agent A and an environment E and an environment state s, the agent is performing an action α, to which the environment responds with a reward r. The agent learns the policy (a map between states and actions), which maximizes the reward.

We use Deep Deterministic Policy Gradient Algorithm (DDPG Algorithm) [17], which is especially suitable for continuous state spaces and continuous action spaces, which is our situation. It is an actor-critic method, consisting of four neural networks: one for learning the policy, one for learning the value function and two as fixed target neural networks.

8. Experimental settings

8.1. Parallelized Powell's Algorithm

We start n different Powell's searches, where n = 1, 50, 100, 300 with well-chosen starting points. The n starting points for each run are selected based on their quality and enforcing diversity by using two diversity measures, one based on Euclidean distance and the other based on angles as described in the Methodology section. Each widened Powell's search is run 20 times. The number of iterations, when generating the starting points for which improvement is not seen, k, is set to 5. The number of iterations of the Powell's method is the default one. The Powell's method from scipy.optimize package is used, in the minimize function, with its default standard settings. The diversity measure threshold for modified Euclidean distance is set to 0.1. The diversity measure threshold for diversity based on angle similarity is set to 0.1.

8.2. Reinforcement learning

To implement the DDPG Algorithm we use the package stable-baselines [18], OpenAI Gym [19].

The observation space was defined as a continuous 819-dimensional box with the first 413 dimensions being bounded by intervals $[0, \pi/2]$ and dimensions from 414 to 819 are bounded by intervals $[0, 2\pi]$. The action space is the same as the observation space. Each step consists of performing only five iterations of the Powell's search method and assigning a reward. The reward is a weighted difference between the geometric quality measure $|\det Q|$ and the penalty, which is based on the number of steps (#st). The penalty was introduced to enforce a faster convergence. Namely, the reward = $|\det Q| - \#st/1000$. The actor, critic and the target networks are implemented as fully connected, simple MultiLayered Perceptron (MLP) networks

with two hidden layers each with 64 neurons. The input layer is of the dimension of the observation space (819) and the output layer has the same size (819) and is fully connected. Ornstein-Uhlenbeck noise is added to the actions to facilitate the training. 350 training steps were performed. The learning rate chosen was 0.0001 for actor and 0.001 for critic with soft update of target set 10^{-3}, the size of the replay buffer was 10^7, gamma discount was 0.99, weight decay set to 10^{-5} batch size 128.

9. Results

Fig. 2 shows the results from Widening of the Powell's method with diversity measure based on the modified Euclidean distance, as described in the Section 6. The box plot for $n = 1$ actually presents the regular Powell's method and we contrast it to the parallel Powell's results. Fig. 3 shows the results from Widening of the Powell's using distance measure based on angle similarity, as described in the Section 6. Again, the boxplot for $n = 1$ represents the plot of the linear Powell's method and it is contrasted with the results obtained by the parallel methods. As expected, the greater the number of parallel searches, the better the obtained result, due to the better exploration of the search space. Fig. 3 shows the results from the reinforcement learning of the already trained algorithm.

Both diversity measures reach a similar level of model quality, even though they both have different reasonings behind them. The quorum with the highest performance, discovered has $|\det Q| = 0.00253$. With reinforcement learning one can see that the results obtained are all of very high quality and very close together in terms of performance (see Fig. 3, the box of the box plot is very flat). This means that the reinforcement method learns how to obtain good solutions after appropriate training and at each step gets another high performing solution. The parallel Powell′s method (Widening) simply explores many different paths in parallel in order to find the best possible solution.

9.1. Structure of the solutions

First, from our analysis, it is obvious that for all good solutions, the Q_j have pairwise angles close to 90°. The maximal quorum, which would be a quorum of equiangular vectors, where all angles are 90° cannot be achieved in principal. However, all angles are very close to 90° compared to the angles between vectors of badly performing quorums. Table 1 shows maximum, minimum, and mean of all angles formed by top quality solutions contrasted with the angles formed by vectors from a bad quality solution.

It can be seen that the size of the angles between vectors of well performing solutions (quorum with a large $|\det Q|$) are consistently good, and the size of the angles between vectors of badly performing solutions – consistently small.

Secondly, we want to investigate the best performing quorums for existing symmetries. In [11], we discovered for $d = 3, 4$ that the optimal solutions had many repeating angles. In fact, each of the discovered angles was repeated many times within a given solution.

Here we are interested in whether within one solution there are common angle patterns between vectors and what is the difference in this respect between well performing and badly performing solutions. Given a vectors Q_i and Q_j, $j \neq i$, from quorum Q we are interested in the intersection of the two sets of angles S_i, S_j, which Q_i and Q_j make with the respective other vectors from quorum Q. In Table 2, we can see $S_i \cap S_j$ for top solutions as well as for badly performing solutions. The table shows the mean, the minimum, and the maximum of $S_i \cap S_j$ taken over all possible combinations of $j \neq i$. It is clear that the good solutions have more angle patterns repeated within one quorum, which implies complex types of symmetrical substructures within the top solutions.

Additionally, we are interested in the common angles formed by the projectors of two quorums. Namely, given two quorums $Q^{(1)} = \{Q'_1, \ldots, Q'_{63}\}$ and $Q^{(2)} = \{Q''_1, \ldots, Q''_{63}\}$ we are interested in the intersections of all possible S'_i, S''_j, where S'_i is the set of angles formed by $Q'_i \in Q^{(1)}$ with all other projectors from $Q^{(1)}$ and S''_j is the set of all angles formed by $Q''_i \in Q^{(2)}$ with the other elements of $Q^{(2)}$. Table 3 shows the mean minimum and maximum of such pairwise intersections between two high-quality quorums and two low-quality quorums. Clearly, from the results we can see that highly performing solutions have similarity in angles between quorum projectors, and badly performing solutions do not have similarities between the angles formed by their projectors.

Lastly, we want to investigate the distance between very highly performing solutions. This will give us information about the landscape of the solution space. Here, for the analysis of the results, we apply a different sorting procedure than previously for the diversity criterion in the Widening. We start with the first element of the first quorum and match it to the element from the second quorum that has the shortest distance to it, for the second element from the first quorum we then search for the closest one among the remaining 62 elements of the second quorum and so on. This still means that we might not find the sorting that provides the shortest distance overall, but it should provide a good idea how far apart two quorums are. The distances given in Table 1 are the sum over the distances of the matched elements of the first and the second quorum divided by 63. Again, we compare the distance between two randomly selected quorums and the distance between highly performing solutions. The distance between the highly performing solutions is greater than that of the randomly selected ones, which hints at the existence of multiple peaks in the search space.

Table 1. Euclidean distance

Characteristics for comparison between two sets	High-ranking set	Random set
Mean set quality	0.002474	2.5357×10^{-63}
Mean set distance	1.0008	0.77012

This implies that the search space of potential solutions has a complex landscape with more than one peak. Clearly, however, if one takes the invariance with regard to angles between projectors of a given quorum, the similarity between highly performing quorums is significantly greater than the similarity between randomly chosen quorums, which perform badly. This shows that very particular structure of

the solutions must be in place in order for them to perform well, regardless of their position in the Euclidean space.

Table 2 shows investigation of common angle patterns within one quorum. These results are focused on looking for structures that exist in quorums, which have high quality with respect to our quality measure and do not exist in solutions, which do not perform well in terms of our quality measure. It shows mean values of the maximal number of common angles that each projector forms with other projectors, the minimal number of common angles shared between projectors, and the mean number of common vectors. The results are investigated for two sets of quorums, one which consists of high-performing solutions, and another which consists of badly-performing solutions. The average quality of the two sets of quorums is also shown in the table.

Table 2. Intersections within a quorum

Characteristics for comparison between two sets	High-ranking set of quorums	Random set of quorums
Mean set quality	0.002474	2.5357×10^{-63}
Mean of maximal number of common angles per projector within a quorum	23.667	7.333
Mean of minimal number of common angles per projector within a quorum	9.952	0.0
Mean of the number of common angles per projector within a quorum	18.742	4.586

Table 3. Common angles which occur in two quorums

Characteristics for comparison between two sets	High-ranking set of quorums	Random set of quorums
Mean set quality	0.002474	2.5357×10^{-63}
Mean of maximal number of common angles per projector between two quorums	24.667	8.0
Mean of minimal number of angles forms with vectors from quorum 1 that can be found also in quorum 2 (per projector)	8.645	0.0
Mean of the number of common angles per projector between two quorums	19.323	4.726

We can see that for solutions, which perform well the similarity of angles is very high compared to the solutions which do not perform well. Additionally, the common angle patterns for a projector within its quorum are almost the same number as the common angle patterns between a projector and another quorum. This discloses similarity in the structure and in the symmetry patterns.

Table 4. Size of angles

Characteristics for comparison between two sets	High-ranking set of quorums	Random set of quorums
Mean set quality	0.002474	2.5357×10^{-63}
Mean of maximal dot product	0.01480	0.7645
Mean of minimal dot product	5.291×10^{-8}	4.984×10^{-5}
Mean of dot product	0.0009049	0.4869

It can be concluded that the angles of random solutions are further from 90° than the angles of top-performing solutions (Figs 2-4).

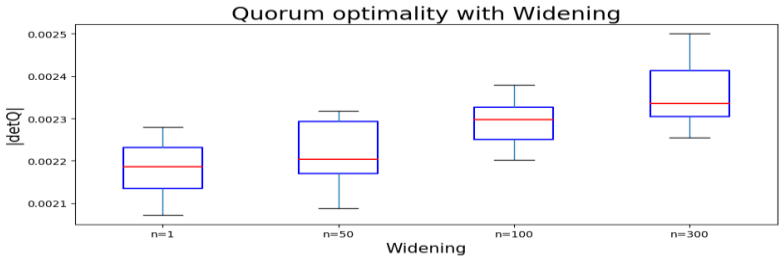

Fig. 2. Quorum optimality with Widening with modified Euclidean distance

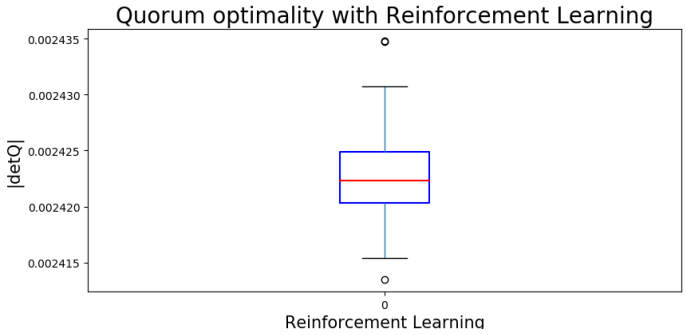

Fig. 3. Quorum optimality with reinforcement learning

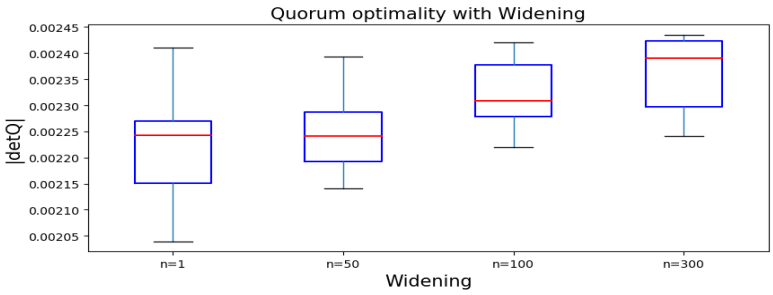

Fig. 4. Quorum optimality with Widening with distance measure based on angle similarity

10. Conclusion

By applying machine learning methods, we were able to find an improved quorum of rank-1 projectors that allows for an efficient quantum state tomography measurement scheme for three qubits compared to previously obtained results by a standard numerical method [14]. The comparison of the obtained solution suggests that the optimal solution is not unique and has some inner symmetries. However, a deeper analysis is needed to completely clarify the mathematical structure, the relation between two distant but equally top-performing solutions, and potentially be able to

construct those solutions for arbitrary dimensions. We expect that the optimal solutions in von-Neumann measurement systems will also possess symmetry, even though not all elements are equiangular to each other unlike the SIC-POVMs for generalized measurements. As the dimensions of the Hilbert space and the parameters increase that may not be the case. Already at 12 dimensions the parameters are over 3000 and Powell's method cannot run in feasible time. Approaches that are more sophisticated will be needed, including analytical and constructive ones, which generalize theoretically the properties of the ideal solutions, discovered by machine learning. Our approach is not limited to rank-1 projections or to any dimension of the Hilbert space. It can be applied to many scenarios where the optimal scheme for quantum state tomography is desired. However, at the rank-1 projection operators it is proven theoretically that the upper bound – the optimal equiangular solution – cannot be reached. The question is how close to this bound can we get in the case of rank-1 projection operators. We intend to proceed with looking for optimal projection operators of rank-1 in higher dimensions and to generalize our findings.

***Acknowledgements*:** This work was partially supported by the Bulgarian National Science Fund via the project number KP-06-PM 32/8, by the Bulgarian Ministry of Education and Science by Grant No DO1-221/03.12.2018 for NCHDC, a part of the Bulgarian National Roadmap on RIs, and by the Zukunftskolleg (University of Konstanz).

References

1. Roos, C. F., G. P. T. Lancaster, M. Riebe, H. Häffner, W. Hänsel, S. Gulde, C. Becher, J. Eschner, F. Schmidt-Kaler, R. Blatt. Bell States of Atoms with Ultralong Lifetimes and Their Tomographic State Analysis. – Phys. Rev. Lett., Vol. **92**, 2004, 220402.
2. O'Brien, J. L., G. J. Pryde, A. G. White, T. C. Ralph, D. Branning. Demonstration of an All-Optical Quantum Controlled-NOT Gate. – Nature, Vol. **426**, 2003, pp. 264-267.
3. Steffen, M., M. Ansmann, R. McDermott, N. Katz, R. C. Bialczak, E. Lucero, M. Neeley, E. M. Weig, A. N. Cleland, J. M. Martinis. State Tomography of Capacitively Shunted Phase Qubits with High Fidelity. – Phys. Rev. Lett., Vol. **97**, 2006, 050502.
4. Foletti, S., H. Bluhm, D. Mahalu, V. Umansky, A. Yacoby. – Nature Physics, Vol. **5**, 2009, pp. 903-908.
5. Zauner, G. Quantendesigns. Doctoral Thesis, 1999. English Translation Published as Quantum Designs: Foundations of a Noncommutative Design Theory. – Int. J. Quantum Inf., Vol. **9**, 2011, No 1, pp. 445-507.
6. Řeháček, J., B.-G. Englert, D. Kaszlikowski. Minimal Qubit Tomography. – Phys. Rev. A, Vol. **70**, 2004, 052321.
7. Renes, J. M., R. Blume-Kohout, A. J. Scott, C. M. Caves. Symmetric Informationally Complete Quantum Measurements. – J. Math. Phys., Vol. **45**, 2004, pp. 2171-2180.
8. Wootters, W. K., B. D. Fields. Optimal State-Determination by Mutually Unbiased Measurements. – Ann. Phys., Vol. **191**, 1989, pp. 363-381.
9. Bodmann, B. G., J. I. Haas. Maximal Orthoplectic Fusion Frames from Mutually Unbiased Bases and Block Designs. – Proc. Amer. Math. Soc., Vol. **146**, 2018, pp. 2601-2616.
10. Rohling, N., G. Burkard. Tomography Scheme for Two Spin-1/2 Qubits in a Double Quantum Dot. – Phys. Rev. B, Vol. **88**, 2013, 085402.
11. Ivanova-Rohling, V. N., N. Rohling. Optimal Choice of State Tomography Quorum Formed by Projection Operators. – Phys. Rev. A, Vol. **100**, 2019, 032332.

12. A k b a r, Z., V. N. I v a n o v a, M. R. B e r t h o l d. Parallel Data Mining Revisited. Better, Not Faster. – In: J. Hollmén, F. Klawonn, A. Tucker, Eds. Advances in Intelligent Data Analysis XI. IDA 2012. Lecture Notes in Computer Science. Vol. **7619**. Berlin, Heidelberg, Springer, 2012, pp. 23-34.
13. I v a n o v a, V. N., M. R. B e r t h o l d. Diversity-Driven Widening. – In: A. Tucker, F. Höppner, A. Siebes, S. Swift, Eds. Advances in Intelligent Data Analysis XII. IDA 2013. Lecture Notes in Computer Science, Vol. **8207**. Berlin, Heidelberg, Springer, 2013, pp. 223-236.
14. I v a n o v a-R o h l i n g, V. N. Communication-Less Strategies for the Widening of Rule Induction. – In: B. Rachev, A. Smrikarov, Eds. Proc. of 19th International Conference on Computer Systems and Technologies, Association for Computing Machinery, New York, 2018, pp. 33-37.
15. I v a n o v a-R o h l i n g, V. N. Neighborhood-Based Strategies for Widening of the Greedy Algorithm of the Set Cover Problem. – In: B. Rachev, A. Smrikarov, Eds. Proc. of 19th International Conference on Computer Systems and Technologies, Association for Computing Machinery, New York, 2018, pp. 27-32.
16. P o w e l l, M. J. D. An Efficient Method for Finding the Minimum of a Function of Several Variables without Calculating Derivatives. – The Computer Journal, Vol. **7**, 1964, pp. 155-162.
17. L i l l i c r a p, T. P., J. J. H u n t, A. P r i t z e l, N. H e e s s, T. E r e z, Y. T a s s a, D. S i l v e r, D. W i e r s t r a. Continuous Control with Deep Reinforcement Learning. – arXiv Preprint, 2015, arXiv:1509.02971.
18. H i l l, A., A. R a f f i n, M. E r n e s t u s, A. G l e a v e, A. K a n e r v i s t o, R. T r a o r e, P. D h a r i w a l, C. H e s s e, O. K l i m o v, A. N i c h o l, M. P l a p p e r t, A. R a d f o r d, J. S c h u l m a n, S. S i d o r, Y. W u. Stable Baselines. – GitHub Repository, 2018. **https://github.com/hill-a/stable-baselines**
19. B r o c k m a n, G., V. C h e u n g, L. P e t t e r s s o n, J. S c h n e i d e r, J. S c h u l m a n, J. T a n g, W. Z a r e m b a. OpenAI Gym. – arXiv Preprint, 2016, arXiv:1606.01540.

Received: 15.09.2020; Second Version: 30.10.2020; Accepted: 4.11.2020